International Journal of Rotating Machinery, 9(2): 97–112, 2003

1023-621X/03 $12.00 + .00
DOI: 10.1080/10236210390147425

Taylor & Francis
Taylor & Francis Group

Identification of Rub and Unbalance in 320 MW Turbogenerators

N. Bachschmid, P. Pennacchi, and A. Vania
Dipartimento di Meccanica, Politecnico di Milano, Milan, Italy

G. A. Zanetta and L. Gregori
Business Unit Generation, CESI-S.p.A., Segrate, Italy

This article presents two experiences of applying a model-based fault-identification method to real machines. The first case presented is an unbalance identification in a 320 MW turbogenerator unit operating in a fossil power plant. In the second case, concerning a machine of the same size but from a different manufacturer, the turbine has been affected by a rub in the sealings. This time, the fault is modeled by local bows. The identification of the faults is performed by means of a model-based identification technique in a frequency domain, suitably modified in order to take into account simultaneous faults. The theoretical background of the applied method is briefly illustrated and some considerations are also presented about the best choice of the rotating speed set of the run-down transient to be used for an effective identification and about the appropriate weighting of vibration measurements at the machine bearings.

Keywords diagnostics, identification, multiple faults, rotordynamics, rub, unbalance

Fault detection and diagnosis in rotating machinery is a very important topic of rotordynamics, and many studies are present in the literature. A complete review of the fault types considered, of the identification methods employed, of the machine types, and of the case histories would require a very long listing, but some useful references can be obtained from Isermann (1995), who has presented a detailed survey of the possible methods that can be employed in general technical processes, for both detection and diagnosis. By restricting the investigation to rotordynamics and limiting the research to the most recent contributions to the literature, two main approaches can be discussed.

In the first approach, the symptoms can be defined using qualitative information based on human operators' experience, which creates a knowledge base that can be used for fault detection. A recent contribution is stated by White and Jecmenica (1999): an expert system can be built up in which various diagnostic reasoning strategies can be applied. Fault-symptom matrixes, fault-symptom trees, if/then rules, or fuzzy logic classifications can be used to indicate, using a probabilistic approach, most probable the type and sometimes also the size and the location of the fault. Also, artificial neural networks can be used to create symptom/fault correlations or to forecast vibrational behavior (Zanetta and Gregori 2001). This qualitative diagnostic approach is widely used in both industrial environments and advanced research work.

The second approach is quantitative and is called the model-based fault-detection method. In this case, a reliable model of the system, or of the process, is used to create the symptom fault correlation, or the input/output relationship. However, this method has many different forms of application. Among the recent contributions to the literature are Mayes and Penny (1999), who introduce a fuzzy clustering method the basis of which is consideration of the vibration data as a high-dimension feature vector; the vibration caused by a particular fault on a specific machine can be considered to be a point in this high-dimension space. This same fault, on a number of similar machines, should produce a cluster of points in the high-dimension space that is distinct from other clusters produced by different faults. The main drawback of this method is the availability of a large database on the dynamic behavior of similar machines, which can emphasize the differences in the responses of similar machines.

In other applications, fault detection can be performed by means of various mode-based approaches, according to the nature of the system under observation.

Received 28 March 2002; accepted 28 March 2002.
This work is partially funded by the MURST (Italian Ministry for the University and Scientific Research) Cofinanziamento, Identificazione di Malfunzionamenti in Sistemi Meccanici for the year 1999.
Address correspondence to Nicolò Bachschmid, Dipartimento di Meccanica, Politecnico di Milano, Via la Masa, 34, I-20158 Milano, Italy. E-mail: nicolo.bachschmid@polimi.it

- In parameter estimation, the characteristic constant parameters of the process or of the components are affected by the fault.
- In state estimation, the constant parameters are unaffected by possible faults and only the state of the system, which is represented by a set of generally unmeasurable state variables (functions of time), is affected by the faults; in this case the model acts as a state observer.
- In parity equations, the faults affect some of the unmeasurable input variables, the parameters are constant, and only the output variables are measured and compared with calculated model output variables.

Therefore, the fault can be identified on the basis of estimation of parameter or state or on the basis of parity equations.

A modal expansion of the frequency-response function of the system, on both the numerical model and the experimental results, is used in Kreuzinger-Janik and Irretier (2000) to identify the unbalance distribution on a test rig rotor. In Markert and colleagues (2000) and Platz and colleagues (2000), the authors present a model and simulated results in which equivalent loads due to the faults (rubbing and unbalances) are virtual forces and moments acting on the linear undamaged system model to generate a dynamic behavior identical to the measured behavior of the damaged system. The identification is then performed by least squares fitting in the time domain. In Edwards and colleagues (2000), a model-based identification in the frequency domain is employed to identify an unbalance on a test rig. A balancing method for nonlinear rotor bearing systems with hydrodynamic bearings, which uses the unbalance response measured at a discrete number of measurement planes is presented in Chen and colleagues (2001) and applied to numerical results. In Patton and colleagues (2001), a complex framework of model-based identification techniques is applied to numerical results of a gas turbine.

A more comprehensive approach, which is able to identify several different types of faults and to discriminate among faults that generate similar harmonic components, has been introduced in Bachschmid and Pennacchi (2000). This method has been experimentally validated on various test rigs and on some real machines (Bachschmid et al. 1999, 2000a, 2000b, 2000c, 2000d; Vania et al. 2001) with many types of faults, such as unbalances, rotor permanent bows, rotor rubs, coupling misalignments, cracks, journal, ovalization, and rotor stiffness asymmetries.

However, in all the literature, with few exceptions, the proposed methods are tested only numerically or on small-scale test rigs. This is normally due to the possibility of easy evaluation of the actual fault, especially as regards unbalance. In this article, a model-based identification method in the frequency domain, able to handle also multiple simultaneous faults, is applied to experimental data of two different 320 MW turbogenerators.

In the first case study, an unbalance identification is presented, even if this case would be more correctly described as a balancing mass identification. Because in this case it was possible to know all the fault-relevant parameters—position, module, and phase—a rather accurate sensitivity analysis was performed; it considered various models of the rotor, tuned on to one of the experimental critical speeds, various rotating speed sets and optimization weights for the vibrations in the bearings of the machine, and also the nodes where these vibrations were measured.

In the second case, a rub on a Low Pressure (LP) turbine is presented. In this case, the location of the rub remained unclear; the most probable location was close to bearing 3 or 4. Only the visual inspection made during the maintenance of the machine that followed its stopping allowed discovery of exactly where the rub had occurred.

MODEL-BASED IDENTIFICATION OF MULTIPLE FAULTS IN THE FREQUENCY DOMAIN

In the model-based identification procedure, input variables are the exciting forces, and output variables are the vibrations. The procedure requires definition of the elements (rotors, bearings, supporting structure) that compose the rotor system. A finite-beam element was assumed for the rotor; the bearings were represented by their stiffness and damping matrixes (therefore, nonlinear oil-film effects are neglected); and several representations were used for the foundation, such as modal, elastodynamic matrix, or lumped springs and dampers. Also, the effect of the faults had to be modeled, and that was done by introducing an equivalent system of external forces and moments. A more detailed analysis is reported in Bachschmid and colleagues (2000b, 2002).

As regards the experimental data, vibration differences between a reference case and the considered case were used. That way, if the system could be considered linear, the vibrational behavior would have been due to the developing fault only. In fact, with reference to the standard matrix equation of the system

$$\mathbf{M}\ddot{\mathbf{x}}_t + \mathbf{D}\dot{\mathbf{x}}_t + \mathbf{K}\mathbf{x}_t = \mathbf{F}(t). \qquad [1]$$

The arising fault causes changes $d\mathbf{M}$, $d\mathbf{D}$, and $d\mathbf{K}$ in mass $\mathbf{M}$, damping $\mathbf{D}$, and stiffness $\mathbf{K}$ matrices. In real machines only a few measuring points along the shaft, usually in the bearings, are available, so it seems difficult to identify these changes from the measurement of vibration $\mathbf{x}_t$. Equation (1) yields

$$(\mathbf{M} + d\mathbf{M})\ddot{\mathbf{x}}_t + (\mathbf{D} + d\mathbf{D})\dot{\mathbf{x}}_t + (\mathbf{K} + d\mathbf{K})\mathbf{x}_t = \mathbf{W} + (\mathbf{U} + \mathbf{M}_u)e^{i\Omega t} \qquad [2]$$

in which the right hand side (rhs) external forces $\mathbf{F}(t)$ are generally unknown, because they are composed by the weight (which is known) and by the original unbalance and bow (which are unknown). If the system is considered to be linear, then the total vibration $\mathbf{x}_t$ can be split in two terms which can be simply superposed:

$$\mathbf{x}_t = \mathbf{x}_1 + \mathbf{x}. \qquad [3]$$

The first vibration vector $\mathbf{x}_1$ is due to the weight $\mathbf{W}$ as well as to the unknown unbalance force $\mathbf{U}\, e^{i\Omega t}$ and unbalance moment $\mathbf{M}_u\, e^{i\Omega t}$. The second term $\mathbf{x}$ is due to the fault. The component $\mathbf{x}$ may be obtained by calculating the vector differences of the actual vibrations $\mathbf{x}_t$ (due to weight, original unbalance, and fault) minus the original vibrations $\mathbf{x}_1$ measured, in the same operating conditions (rotation speed, flow rate, power, temperature, etc.) before the fault occurrence. Recalling the definition of $\mathbf{x}_1$, the pre-fault vibration, following equation holds:

$$\mathbf{M}\,\ddot{\mathbf{x}}_1 + \mathbf{D}\,\dot{\mathbf{x}}_1 + \mathbf{K}\,\mathbf{x}_1 = \mathbf{W} + (\mathbf{U} + \mathbf{M}_u)\, e^{i\Omega t} \qquad [4]$$

which substituted in Equation (2) gives:

$$\mathbf{M}\,\ddot{\mathbf{x}} + \mathbf{D}\,\dot{\mathbf{x}} + \mathbf{K}\,\mathbf{x} = -d\mathbf{M}\,\ddot{\mathbf{x}}_t - d\mathbf{D}\,\dot{\mathbf{x}}_t - d\mathbf{K}\,\mathbf{x}_t \qquad [5]$$

The r.h.s. of Equation (5) can be considered as a system of equivalent external forces, which force the fault-free system to have the change in vibrations defined by $\mathbf{x}$, that is due to the developing fault only:

$$\mathbf{M}\,\ddot{\mathbf{x}} + \mathbf{D}\,\dot{\mathbf{x}} + \mathbf{K}\,\mathbf{x} = \mathbf{F}_f(t) \qquad [6]$$

Using this last approach, the problem of fault identification is then reduced to a force identification procedure with known system parameters, keeping in mind that a particular force system corresponds to each type of fault considered. Since the final goal is the identification of faults, this approach is preferred since only few elements of the unknown fault forcing vector are in reality different from zero, which reduces significantly the number of unknowns to be identified. In fact, the forces that model each fault are considered to be applied in not more than two different nodes along the rotor. If we consider a steady-state situation, keeping in mind that also a slow run down transient can be considered to be a succession of steady-state situations, assuming linearity of the system and applying the harmonic balance criteria from Equation (6), we get, for each harmonic component, the equations:

$$\left[-(n\,\Omega)^2\,\mathbf{M} + in\,\Omega\,\mathbf{D} + \mathbf{K}\right]\mathbf{X}_n = \mathbf{F}_{f_n}(\Omega) \qquad [7]$$

where the force vector $\mathbf{F}_{f_n}$, has to be identified. This force vector could be function of Ω or not depending on the type of the fault. If the presence of several faults (f.i. m faults) is considered, then the force vector $\mathbf{F}_{f_n}$ is composed by several vectors $\mathbf{F}^{(1)}_{f_n}, \mathbf{F}^{(2)}_{f_n}, \ldots,$ $\mathbf{F}^{(m)}_{f_n}$:

$$\mathbf{F}_{f_n}(\Omega) = \sum_{i=1}^{m} \mathbf{F}^{(i)}_{f_n}(\Omega) \qquad [8]$$

Generally the fault identification procedure is started when the vibration vector change exceeds a suitable pre-established acceptance region; in this case it is more likely that the change in the vibrational behaviour is really caused by an impeding fault only. Anyway, multiple faults may occur in real machines; sometimes a bow (due to several different causes) and an unbalance or a coupling misalignment may develop simultaneously. Another case of multiple fault identification can be considered when the reference situation $\mathbf{x}_1$ is not available. Then the arising fault is superposed on the original unbalance and bow distribution. In this case also multiple fault identification may be useful for selecting the developing fault and the original unbalance and bow.

Few spectral components $\mathbf{X}_n$ in the frequency domain (generally not more than three, in the absence of rolling bearings and gears), measured in correspondence with the bearings, represent completely the periodical vibration time history.

Moreover, the kth fault acts on few degrees of freedom (dofs) of the system, so that the vector $\mathbf{F}^{(k)}_{f_n}$ is not a full-element vector; it is convenient represent it by

$$\mathbf{F}^{(k)}_{f_n}(\Omega) = \left[\mathbf{F}^{(k)}_L\right]\mathbf{A}^{(k)}(\Omega) \qquad [9]$$

where $[\mathbf{F}^{(k)}_L]$ is the localization vector, which has all null elements except for the dof to which the forcing system is applied, and $\mathbf{A}^{(k)}(\Omega)$ is the complex vector of the identified defects. The localization vector gives the position of the fault along the rotor and expresses the link between the force fault system and the modulus and phase of the identified fault that has produced it.

Many fault models have been introduced that correspond to common faults that occur in real machines; see, for example, Bachschmid and Pennacchi (2000), Bachschmid and colleagues (2002), and Platz and Markert (2001). For this article, it is sufficient to consider only the unbalance and the rub.

The unbalance has only a $1\times$ revolution component. The complex vector of the general kth fault force system becomes, in this case,

$$\begin{aligned}\mathbf{F}^{(k)}_{f_1} &= \begin{bmatrix}0 & \vdots & 1 & 0 & i & 0 & \vdots & 0\end{bmatrix}^{\mathrm{T}} \cdot (mr)^{(k)}\Omega^2 e^{i\varphi^{(k)}} \\ &= \left[\mathbf{F}^{(k)}_L\right]\mathbf{A}^{(k)}(\Omega)\end{aligned} \qquad [10]$$

where the only elements different from zero are the ones relative to the horizontal and vertical dof of the node j, where the unbalance is supposed to be applied. Note that in this case the fault force system is a function of the rotating speed Ω.

Rub modeling is not as straightforward as unbalance modeling. Often nonlinear effects are present, and characteristic behaviors like the Newkirk effect can be observed (Bachschmid et al. 2001; Kellenberger 1980; Liebich 1998; Vania et al. 2001). In general, rub determines an asymmetrical heating of a symmetrical rotor, which causes an asymmetrical axial strain distribution on the cross-section and the shaft bows. The asymmetrical heating can be localized when it is due to a full annular rub (local bow), or can extend to a certain length of the rotor, as in a generator when a cooling duct is obstructed (extended bow). For diagnostics purposes, a bow can be simulated, generally in a fairly

accurate way, by imposing on the rotor, in only two nodes of the model, a suitable system of rotating and speed-independent bending moments. These generate the same (polarly asymmetrical) strains, the same static deflection and, dynamically, at the operating speed, the total vibration of the shaft. Therefore, in each one of the two nodes of the finite element model (the extremity nodes of the part of the rotor that is affected by the bow) only one rotating moment is applied in order to have an easier identification procedure.

The complex vector of the fault force system $\mathbf{F}_{f_1}^{(k)}$, which simulates the kth bow, and the corresponding $[\mathbf{F}_L^{(k)}]$ and $\mathbf{A}^{(k)}$ become

$$\begin{aligned}\left[\mathbf{F}_L^{(k)}\right] &= \left[0 \;\vdots\; 0 \;\; i \;\; 0 \;\; 1 \;\vdots\; 0 \;\vdots\; 0 \;\; -i \;\; 0 \;\; -1 \;\vdots\; 0\right]^{\mathrm{T}} \\ \mathbf{A}^{(k)} &= M^{(k)} e^{i\varphi^{(k)}}\end{aligned} \qquad [11]$$

where the only elements different from zero are the ones relative to the horizontal and vertical rotational dof of two nodes. However, in this case the diagnostic significance of the identified fault is mainly in its location, whereas the bending moments cannot be used directly because they do not correspond to anything actually measured on the machines. But they can be used to simulate the machine's behavior and compare it with the experimental one.

Finally, Equation (7) can be rewritten, for each harmonic component, in the following way:

$$[\mathbf{E}(n\Omega)]\mathbf{X}_n = \sum_{i=1}^{m} \mathbf{F}_{f_n}^{(i)}(\Omega) = \mathbf{F}_{f_n}(\Omega) \qquad [12]$$

where $[\mathbf{E}(n\Omega)]$ is the system's dynamical stiffness matrix for the speed Ω and for the nth harmonic component. Nowadays, experimental vibration data from real machines (Gregori et al. 2000) are commonly collected by condition-monitoring systems and are available for many rotating speeds, typically those of the run-down transient that, in the large turbogenerators of power plants, occurs with slowly changing speed due to the high inertia of the system, so that actually the transient can be considered as a series of different steady-state conditions. This allows use of these data in the frequency domain. The identification method can be applied for a set of p rotating speeds that can be organized as a vector:

$$\boldsymbol{\Omega} = [\Omega_1 \Omega_2 \cdots \Omega_p]^{\mathrm{T}}. \qquad [13]$$

Then the matrix and vectors of Equation (12) have to be expanded:

$$[\mathbf{E}(n\boldsymbol{\Omega})]\,\mathbf{X}_n = \begin{bmatrix} \mathbf{E}(n\Omega_1) & 0 & 0 & 0 \\ 0 & \mathbf{E}(n\Omega_2) & 0 & 0 \\ \vdots & \vdots & \vdots & \vdots \\ 0 & 0 & 0 & \mathbf{E}(n\Omega_p) \end{bmatrix} \begin{bmatrix} \mathbf{X}_n \\ \mathbf{X}_n \\ \vdots \\ \mathbf{X}_n \end{bmatrix}$$

$$= \begin{bmatrix} \sum_{i=1}^{m} \mathbf{F}_{f_n}^{(i)}(\Omega_1) \\ \sum_{i=1}^{m} \mathbf{F}_{f_n}^{(i)}(\Omega_2) \\ \vdots \\ \sum_{i=1}^{m} \mathbf{F}_{f_n}^{(i)}(\Omega_p) \end{bmatrix} = \mathbf{F}_{f_n}(\boldsymbol{\Omega}) \qquad [14]$$

From a formal point of view, it is unimportant to consider one or p rotating speeds in the identification. The fault vector is the sum of all the faults that affect the rotor, as stated in Equation (8). Matrix $[\mathbf{E}(n\boldsymbol{\Omega})]$ can be inverted and Equation (12) becomes

$$\mathbf{X}_n = [\mathbf{E}(n\boldsymbol{\Omega})]^{-1} \cdot \mathbf{F}_{f_n}(\boldsymbol{\Omega}) = \boldsymbol{\alpha}_n(\boldsymbol{\Omega}) \cdot \mathbf{F}_{f_n}(\boldsymbol{\Omega}) \qquad [15]$$

where $\boldsymbol{\alpha}_n(\boldsymbol{\Omega})$ is the inverse of $[\mathbf{E}(n\boldsymbol{\Omega})]$. Reordering in a suitable way the lines in Equation (15) by partitioning the inverse of the system's dynamic stiffness matrix and omitting from $\boldsymbol{\alpha}_n$ and $\mathbf{F}_{f_n}$ the possible dependence on $\boldsymbol{\Omega}$ for conciseness, we obtain

$$\begin{cases} \mathbf{X}_{B_n} = \boldsymbol{\alpha}_{B_n} \cdot \mathbf{F}_{f_n} \\ \mathbf{X}_{A_n} = \boldsymbol{\alpha}_{A_n} \cdot \mathbf{F}_{f_n} \end{cases} \qquad [16]$$

where $\mathbf{X}_{B_n}$ is the complex amplitude vector representing the measured absolute vibrations in correspondence with the measuring sections, and $\mathbf{X}_{A_n}$ is the vector of the remaining dof of the rotor system model.

Using the first part of Equation (16), the differences $\boldsymbol{\delta}_n$, between calculated vibrations $\mathbf{X}_{B_n}$ and measured vibrations $\mathbf{X}_{Bm_n}$ can be defined, for each harmonic component, as

$$\boldsymbol{\delta}_n = \mathbf{X}_{B_n} - \mathbf{X}_{Bm_n} = \boldsymbol{\alpha}_{B_n} \cdot \mathbf{F}_{f_n} - \mathbf{X}_{Bm_n} \qquad [17]$$

The number of equations n_E (the number of measured dofs) is lower than the number n_F (the number of dofs in the complete system model), which is also the number of elements of $\mathbf{F}_{f_n}$. But, as noted before, $\mathbf{F}_{f_n}$ becomes a vector with many null elements, even if the fault is single, so the number of unknown elements in $\mathbf{F}_{f_n}$ is smaller than the number of equations. The system, therefore, does not have a single solution for all the equations and it is necessary to use the least squares approach in order to find the solution (identified fault) that minimizes the differences that are calculated for all the different rotating speeds that have been taken into consideration. Moreover, it is useful to introduce also a weighting of each of the measured vibrations so as to give less relevance to those that are not significant or can be affected by errors.

A scalar relative residue may be defined by the root of the ratio of the squared $\boldsymbol{\delta}_n$ divided by the sum of the squared measured vibration amplitudes $\mathbf{X}_{Bm_n}$:

$$\delta_{r_n} = \left(\frac{[\boldsymbol{\alpha}_{B_n} \cdot \mathbf{F}_{f_n} - \mathbf{X}_{Bm_n}]^{*\mathrm{T}} [\boldsymbol{\alpha}_{B_n} \cdot \mathbf{F}_{f_n} - \mathbf{X}_{Bm_n}]}{\mathbf{X}_{Bm_n}^{*\mathrm{T}} \mathbf{X}_{Bm_n}} \right)^{1/2}. \qquad [18]$$

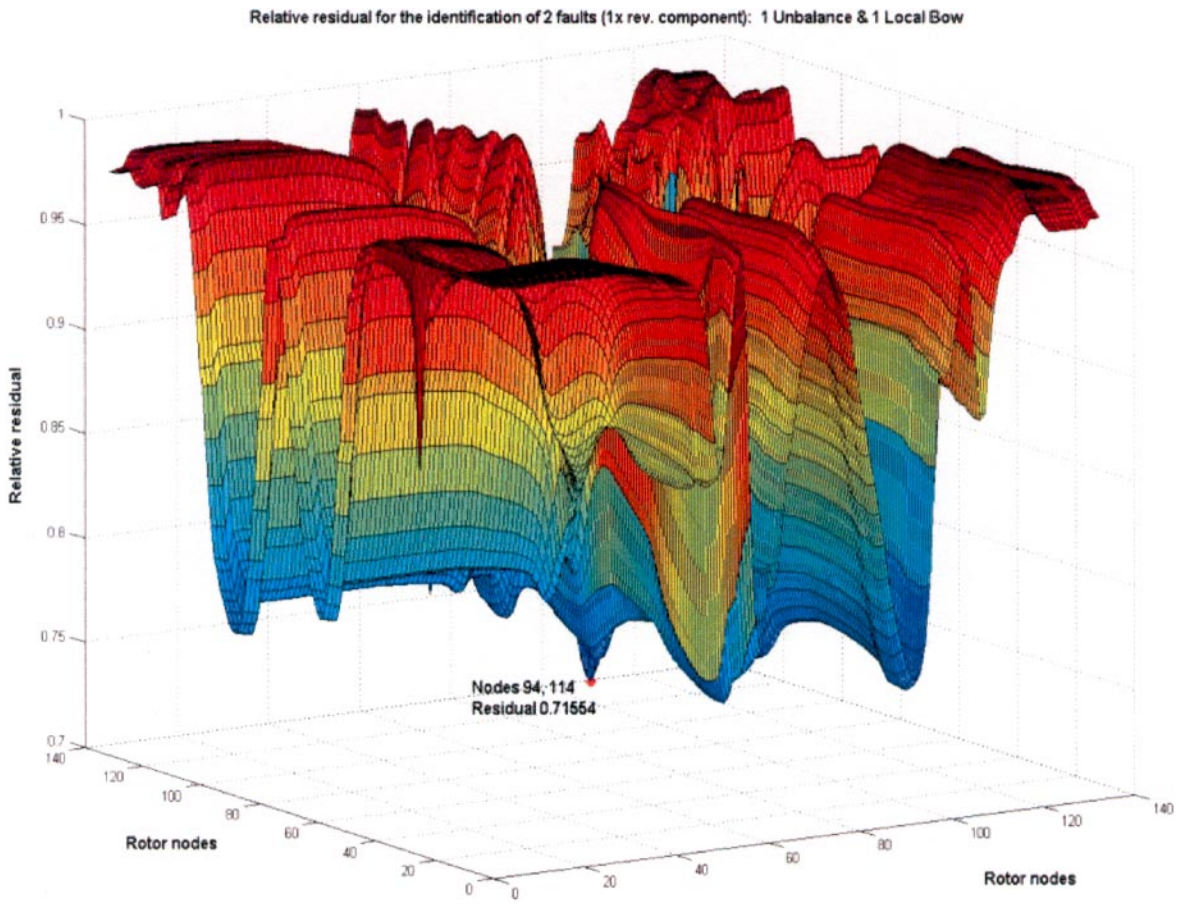

FIGURE 1
Residue surface.

By means of the hypothesis of localization of the fault, the residue is calculated for each possible node of application of each defect. This implies that if we indicate with z_k the abscissa along the rotor in correspondence to the kth fault among m faults, the relative residue in Equation (18) is a surface in a $\mathbb{R}^{m+1}$ space; in other terms,

$$\delta_{r_n} = f(z_1, z_2, \ldots, z_k, \ldots, z_m). \qquad [19]$$

The place where the residue reaches its minimum—that is, the minimum of the surface in Equation (19)—is the most probable location of the fault. Figure 1 shows a sample of a residue surface in a case of two faults.

The corresponding values of $\mathbf{F}_{f_n}$ give the modulus and the phase of the identified faults. The identification procedure is implemented by the code ADVANT (automatic diagnosis by vibration analysis of turbogenerator rotors), which has been used in the case studies presented in the paper. The relative residue also gives an estimate of the quality of the identification, because the closer to zero its value, the better the identified fault corresponds to the actual one; this follows easily from analysis of Equation (18).

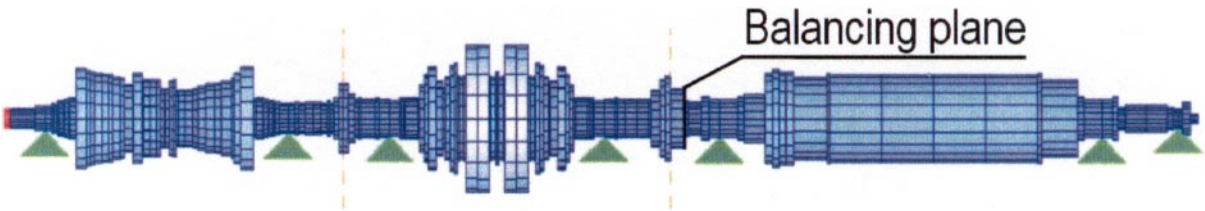

FIGURE 2
320 MW turbogenerator model used for unbalance identification.

IDENTIFICATION OF UNBALANCE ON A 320 MW TURBOGENERATOR

The first case presented concerns a 320 MW turbogenerator (Fig. 2) composed of two turbines, a high-intermediate pressure (HP-IP) and an LP, and a generator connected by rigid couplings, on seven oil-film bearings, of which those on the HP-IP turbine are tilting pads, those on the LP turbine are cylindrical, the first two on the generator are lemon-shaped, and the last two are tilting pads; it is operating at a rated speed of 3000 rpm. The rotor, which is about 28 m long and has a mass of about 131 tons (the HP-IP turbine 26 t , the LP turbine 53 t, and the generator 52 t), has been modeled by 167 beams. The bearing stiffness and damping coefficients are defined for several rotating speeds in the range 300–3000 rpm, and the foundation is modeled by mass, spring, and damper systems whose parameters are defined for several rotating speeds, also in the range 300–3000 rpm.

The ADVANT code has been employed on this machine to identify a force due to a mass added for balancing, which was performed by adding a 630-g mass at a radial distance of 406 mm from the rotating axis, thus producing an unbalance of 0.256 kg on the coupling between the LP turbine and the generator, on the coupling face toward the generator. The corresponding model node is 132, and, considering the ADVANT code angle convention, the phase is -22.5° (Fig. 3).

The experimental data sets available for this turbo group are related to four different run-downs of the machine in normal operating conditions, two of which are considered reference cases, as they were made before the balancing, and the other two of which are the faulty cases, as they were made after the balancing. Before using them for the identification, the data were screened, taking into account the values of the vibration differences on all the possible combinations between the reference and the faulty cases. Then, only four typical rotating speeds were considered (1500, 2000, 2500, and 3000 rpm) and were equally spaced in the frequency range in which the system response to unbalance is significant; the effect of the balancing mass at lower rotating speed could not be appreciable. The analysis has given following results in terms of percentage of deviation from the average of the four vibration differences:

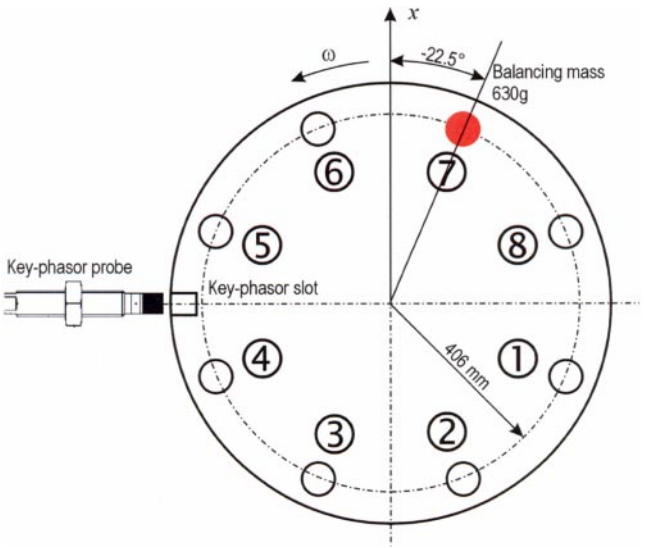

FIGURE 3
Balancing mass position.

- Maximum absolute deviation on all the vibrations (normalized on bearing number 1, vertical vibration): 296%
- Minimum absolute deviation on all the vibrations (normalized on bearing number 5, vertical vibration): 1.34%
- Maximum average deviation on all the vibrations and all the differences: 168%
- Minimum average deviation on all the vibrations and all the differences: 6%
- Average deviation on all the vibrations and all the differences: 48%
- Average deviation on all the vibrations of bearings numbers 1, 2, and 7 and all the differences: 83%
- Average deviation on all the vibrations of bearings numbers 3, 4, 5, and 6 and all the differences: 22%

This analysis suggests giving a small weight to or not considering at all the data of bearings 1, 2, and 7 and indicates that the expected result of the identification cannot be considered an

TABLE 1
Unbalance Case Experimental and Model Critical Speeds for the Turbines and the Generator

	HP-IP turbine				LP turbine				Generator			
	1st		2nd		1st		2nd		1st		2nd	
	H	V	H	V	H	V	H	V	H	V	H	V
Experimental	1560	1580	>3000	>3000	1230	1770	2350	?	825	?	2175	2565
Model A	1830	1830	3850	3850	1570	1470	3380	3230	1000	980	2710	2620
Model B	1600	1640	4470	4490	1480	1690	3130	3530	900	1010	2150	2550
Model C	1580	1630	4450	4490	1260	1690	2390	2850	860	1010	2170	2560
Model D	1570	1630	4450	4490	1260	1690	2490	3390	870	1010	2170	2550
Model E	1580	1620	4440	4490	1260	1680	2370	3310	870	1010	2170	2550

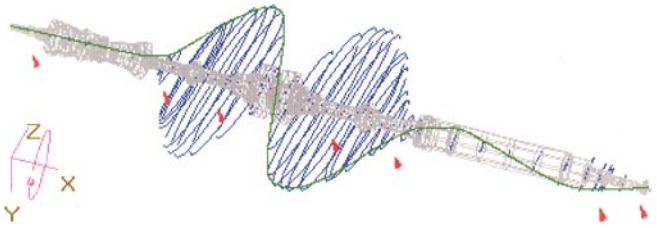

FIGURE 4
320 MW turbogenerator, model of mode shape corresponding to LP turbine, second critical speed in horizontal direction.

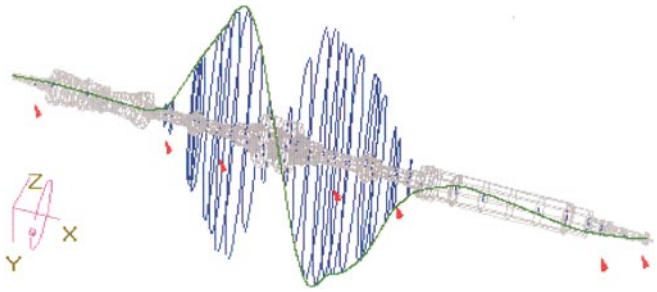

FIGURE 5
320 MW turbogenerator, model of mode shape corresponding to LP turbine, second critical speed in vertical direction.

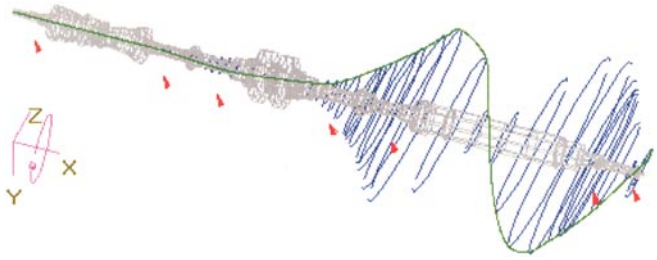

FIGURE 6
320 MW turbogenerator, model of mode shape corresponding to generator, second critical speed in horizontal direction.

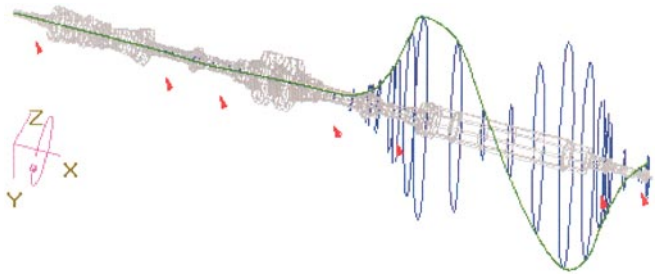

FIGURE 7
320 MW turbogenerator, model of mode shape corresponding to generator, second critical speed in vertical direction.

TABLE 2
Experimental and Model Critical Speeds for the Mode with Maximum on Coupling LP Generator

	H	V
Experimental	>3000	>3000
Model A	>5000	>5000
Model B	4220	>5000
Model C	4170	>5000
Model D	4150	>5000
Model E	4140	>5000

absolute value but should be related to the quality of the experimental data. In this case, by excluding the data of bearings 1, 2, and 7, the quality can be measured by the 22% of the average deviation in all the vibrational differences.

Then the rotor machine model was tuned, using the DYNARO (dynamic analysis of rotors) code, and various models were prepared. By considering the experimental results (Table 1), it was not possible to identify exactly all the critical rotating speeds on the turbogenerator under consideration. In particular, the second critical speed of the LP turbine in the vertical direction, which on this kind of machine is in the range of 10%, more or less, of the operating speed, was not identified. Also the critical speeds in the horizontal and vertical directions of the second mode of the HP-IP turbine were not identified. Moreover, it is worth noting that the frequency response in the range of 2500–3000 rpm is due primarily to a mode with a maximum on the coupling between the LP turbine and the generator, whose critical speed is higher than 3000 rpm.

Five different models of the rotor were considered; they are different from each other in terms of the critical speeds of the rotor sections (see Table 1) and sometimes of the modal dampings. Model A had already been used in previous analyses, because it is one of the most common in Italian power stations and had not been tuned at all before being implemented in ADVANT. Model B through model E are more carefully tuned based on the experimental data and differ especially in the values of the second critical speeds of the LP turbine. As an example, Figures 4 through 7 show some mode shapes for model E obtained by DYNARO. Table 2 reports also the critical speed values corresponding to the mode (Figure 8) that has

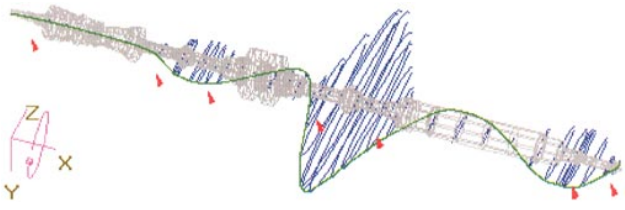

FIGURE 8
320 MW turbogenerator, model of mode shape corresponding to mode with maximum on the coupling between the LP turbine and the generator.

a maximum on the coupling between the LP turbine and the generator.

As regards the choice of the rotating speed set at which the corresponding measures are used for the identification, the above mentioned set of 1500, 2000, 2500, and 3000 rpm—all the speeds available—were employed.

Several identifications have been preformed using ADVANT, considering different models of the rotor, weights of the experimental data, rotating speed sets, and measuring planes. As regards the latter aspect, the element of the model in which the experimental measures are considered to have been taken, two hypotheses have been introduced: in the first case, the position of the measuring plane is in the middle of the bearing; in the second case, it is as close as possible to the actual measuring plane.

The unbalance identification results are shown in Table 3, where the weights used for the horizontal and vertical measures in the bearings are also reported. The differences in the amplitude between the balancing mass and the identified unbalance are normalized to the balancing mass value, while the phases are normalized to 180 degrees (a 100% error is a 180-degree phase error).

As an example, Figure 9, shows the residues along the rotor for the last case in Table 3, with model E. Note the sharp minimum corresponding to the node of the identified fault.

The comparisons between experimental and calculated results for bearings 3, 4, 5, and 6, using the parameters of the identified fault in the last case, are shown in Figures 10 through 13. The results can be deemed good in the vertical direction, whereas in horizontal direction the calculated results generally underestimate the amplitude corresponding to the second critical speed, even with good behavior on the phase.

The results summarized in Table 3 can be considered acceptable, in particular, the use of the no-tuned model A, which allowed the position of the fault and its phase to be identified correctly, even if the amplitude was overestimated; the use of few measuring points (as in the last case, model D) produces completely wrong results.

Better results could have been obtained by means of a more accurate tuning of the models that was not possible due to the difficulty of determining some of the critical speeds in the experimental data. Anyway, the position of the fault is always identified

TABLE 3
Unbalance Identification Results

Model	Rotating speed set (rpm)	Weights on the bearing measure							Measuring section	Node	Amplitude (kg)	Δ amplitude	Phase	Δ phase	Residue
			1	2	3	4	5	6	7							
Actual unbalance											132	0.256		−22.5°		
Model A	All the available	H	1	1	1	1	1	1	1	Brg.	132	0.720	181%	−28.4°	−3%	0.607
		V	1	1	1	1	1	1	1							
Model B	All the available	H	1	1	1	1	1	1	1	Brg.	131	0.290	13%	−35.8°	−7%	0.710
		V	1	1	1	1	1	1	1							
Model B	1500, 2000, 2500, 3000	H	0.5	0.5	1	1	1	1	0.5	Brg.	131	0.535	109%	−36.7°	−8%	0.600
		V	0.5	0.5	1	1	1	1	0.5							
Model C	All the available	H	0.1	0.1	1	1	1	1	0.1	Brg.	133	0.143	−44%	−15.0°	4%	0.810
		V	0.1	0.1	1	1	1	1	0.1							
Model C	1500, 2000, 2500, 3000	H	0.1	0.1	1	1	1	1	0.1	Brg.	132	0.366	43%	−34.2°	−7%	0.672
		V	0.1	0.1	1	1	1	1	0.1							
Model D	All the available	H	0	1	1	1	1	1	0	M.s.	133	0.212	−17%	−27.5°	−3%	0.685
		V	0	1	1	1	1	1	0							
Model D	1500, 2000, 2500, 3000	H	0.1	0.1	1	1	1	1	0.1	Brg.	132	0.385	50%	−36.8°	−8%	0.657
		V	0.1	0.1	1	1	1	1	0.1							
Model D	1500, 2000, 2500, 3000	H	0.1	0.1	1	1	1	1	0.1	M.s.	132	0.339	32%	−39.8°	−10%	0.588
		V	0.1	0.1	1	1	1	1	0.1							
Model D	1500, 2000, 2500, 3000	H	0.1	1	1	1	1	1	0.1	M.s.	133	0.358	40%	−40.7°	−10%	0.567
		V	0.1	1	1	1	1	1	0.1							
Model D	1500, 2000, 2500, 3000	H	0	0	0	0	0	0	0	M.s.	50	0.0967	−62%	−42.6°	−11%	0.704
		V	0	1	1	1	1	1	0							
Model E	All the available	H	0	1	1	1	1	1	1	M.s.	133	0.188	−27%	−23.8°	−1%	0.740
		V	0	1	1	1	1	1	1							
Model E	1500, 2000, 2500, 3000	H	0	1	1	1	1	1	0	M.s.	132	0.363	42%	−39.3°	−9%	0.560
		V	0	1	1	1	1	1	0							

Brg, measuring plane in the middle of the bearing: M.s., measuring plane as close as possible to the actual one.

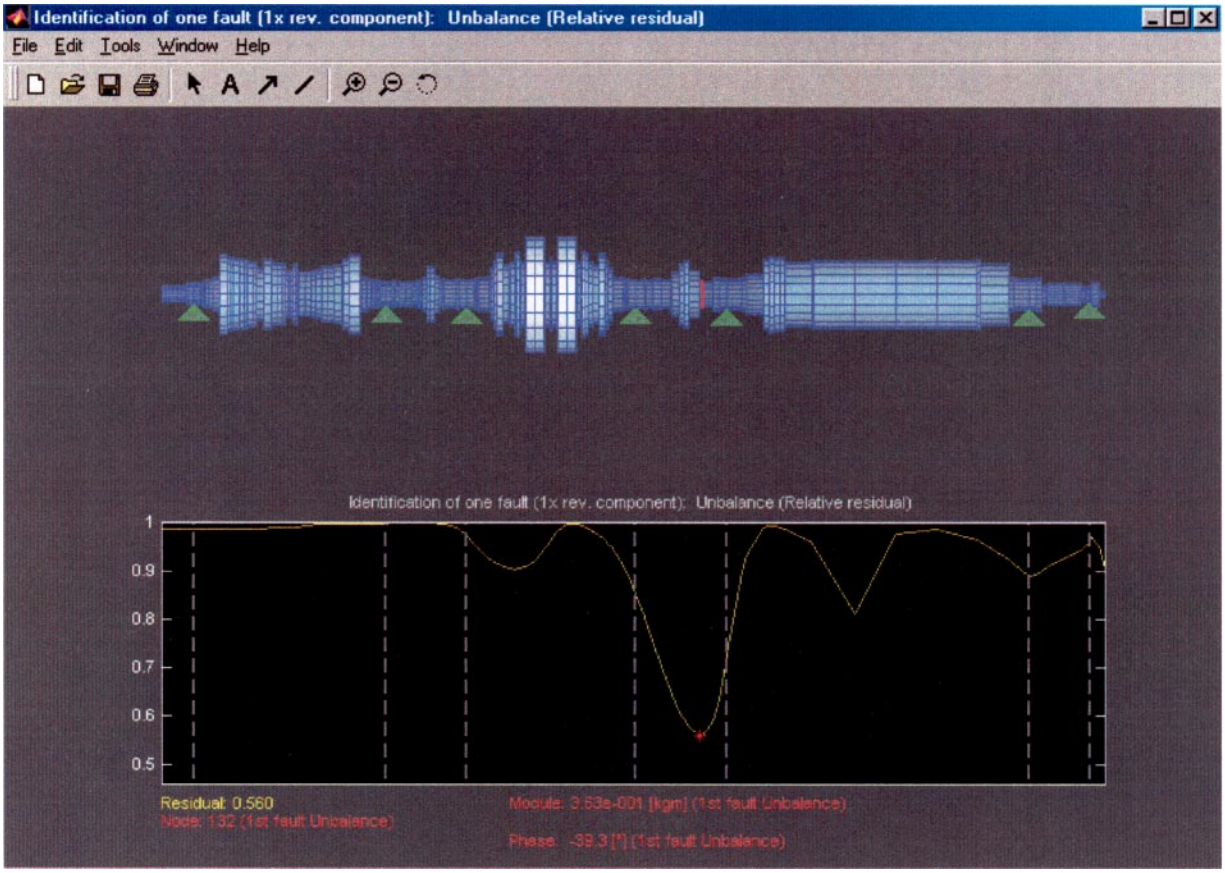

FIGURE 9
Unbalance identification; residue along the rotor as calculated by ADVANT.

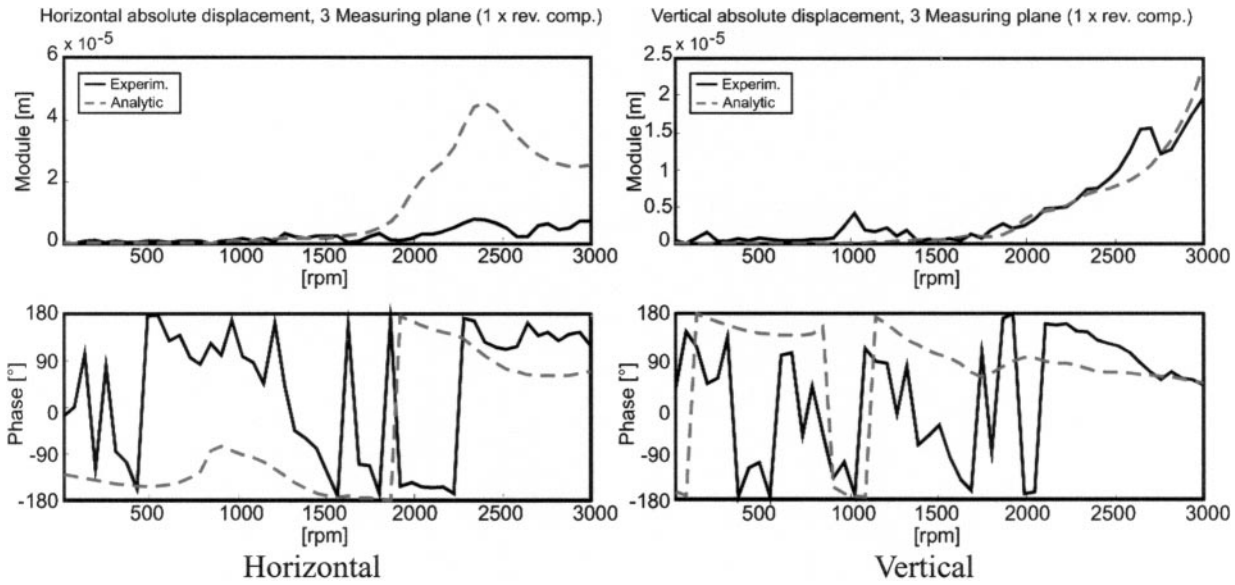

FIGURE 10
Unbalance identification; comparison between experimental and calculated results for bearing 3.

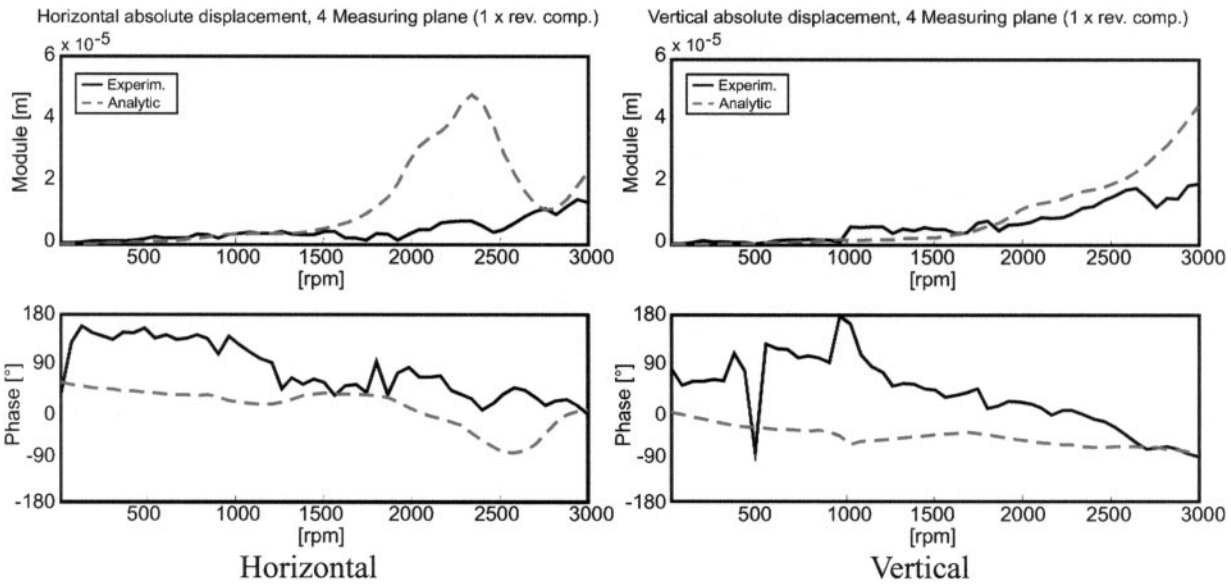

FIGURE 11
Unbalance identification; comparison between experimental and calculated results for bearing 4.

with high accuracy, and the error in the phase is never greater than 20 degrees. The identified amplitude results are more sensitive to the model-tuning and the rotating speed set, but the error is acceptable from an engineering point of view.

ROTOR RUB IDENTIFICATION IN A 320 MW TURBOGENERATOR

The second case concerns another 320 MW turbogenerator (Fig. 14) composed of two turbines, an HP-IP and a LP, and a generator connected by rigid couplings, on seven oil-film bearings of which those on the HP-IP turbine are bilobed and the others lemon-shaped, operating at a rated speed of 3000 rpm. The rotor, which also in this case is about 28 m long and has a mass of about 120 t (the HP-IP turbine, 22 t; the LP turbine, 52 t; and the generator, 46 t), has been modeled by 132 beams. The bearing stiffness and damping coefficients are defined for rotating speeds of 1000, 2000, and 3000 rpm, while the foundation is modeled by mass, spring, and damper systems whose parameters are defined only at 3000 rpm and therefore are

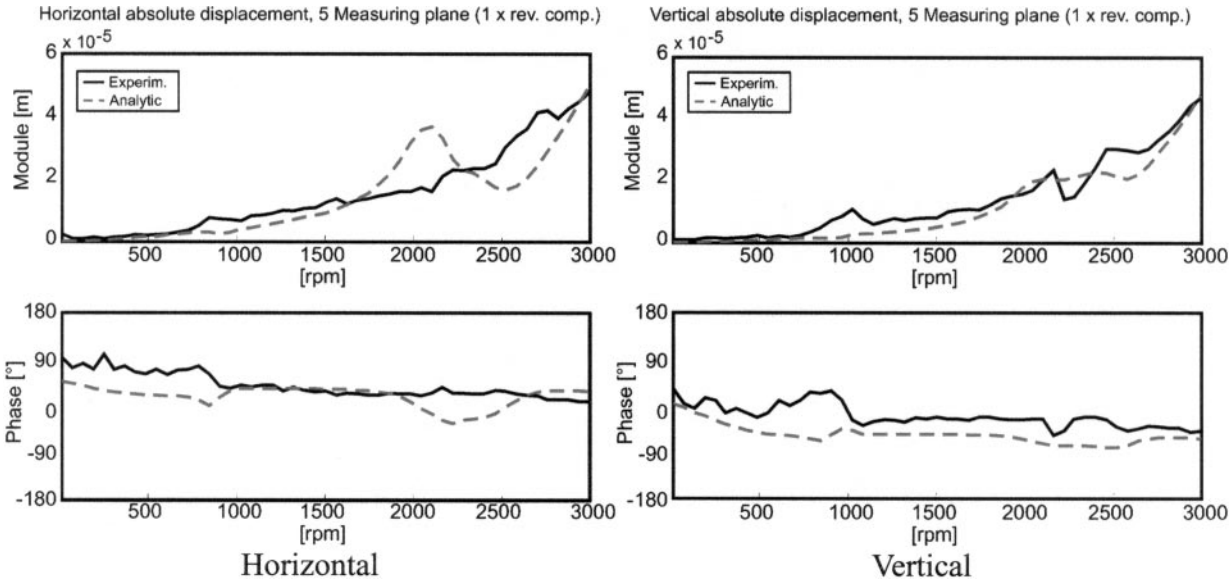

FIGURE 12
Unbalance identification; comparison between experimental and calculated results for bearing 5.

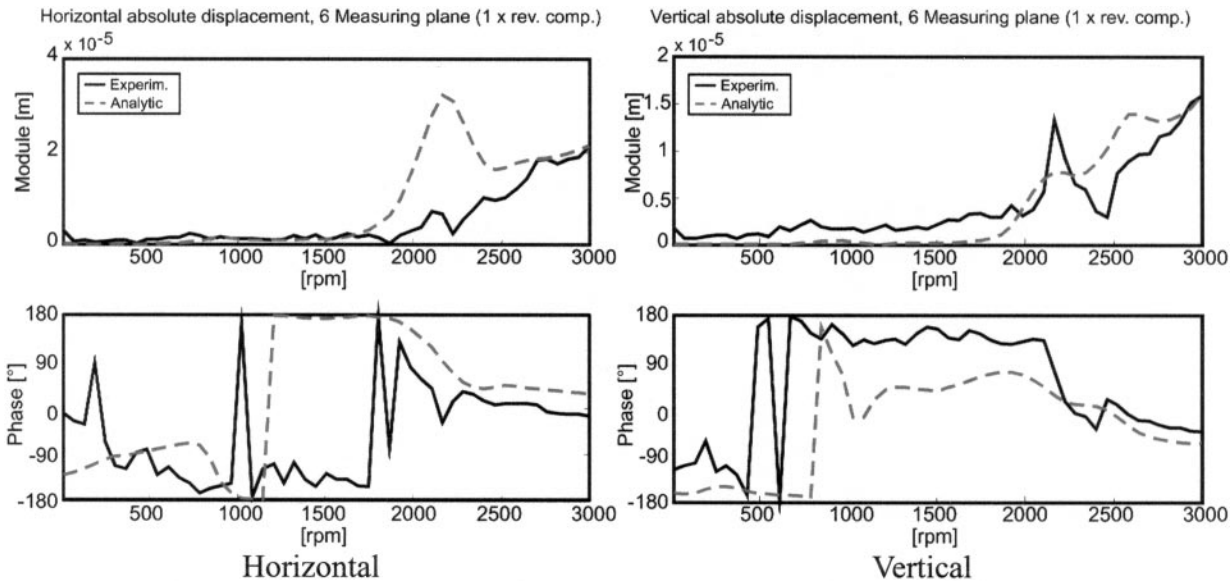

FIGURE 13
Unbalance identification; comparison between experimental and calculated results for bearing 6.

considered to be constant for all the rotating speeds used for the identification.

The available experimental data are relative to two machine run-downs, of which the first was considered the reference case and the second the consequence of a suspected rub. Analysis of the latter data indicated as the possible rubbing sections the two sealing zones close to both last stages of the LP turbine (Fig. 14).

Also in this case it was not possible to fine-tune the rotor model. In fact, neither the analyses of the two experimental data sets on this turbogenerator nor those of a similar turbogenerator in another plant allowed correct identification of all the critical speeds, as reported in Table 4. This notwithstanding, by combining these data, a model that can reproduce approximately the average speeds of the two similar turbogenerators has been implemented in ADVANT. No tuning was made on the modal dampings of the model.

First, an identification of a single local bow, corresponding to a rub, was performed.

The results are reported in Figure 15 and shows that the hypothesis of a rub in the last stage of the LP turbine, close to bearing 4, was confirmed. Figure 16 shows the approximate positions of the sealings on the LP turbine and it can be easily confirmed that sealing 4 is in the identified position of the rub.

Then, the identification of two local bows, looking also for a possible rub in the last stage of the LP, close to bearing 3, was not successful because the second local bow was located on the generator whereas the first was practically in the same section as before (Fig. 17) even if in this case, the residue value was less than that of previous identification.

A further identification was made in looking for a local bow (a rub) and an extended bow on a certain length of the rotor. The results, shown in Figure 18, show that the rub was again identified in sealing 5, close to the last stage of LP turbine, but the LP turbine also presents an extended bow. Also, in this case the residue value is less than that of a single local bow. Figures 19 and 20 show the comparison between experimental vibrations and calculated vibrations on the bearings of the LP turbine. The agreement can deemed good, considering that the model is not tuned and that the quality of the experimental data is fair. The final validation of the identification procedure was obtained by the result of the visual inspection during the

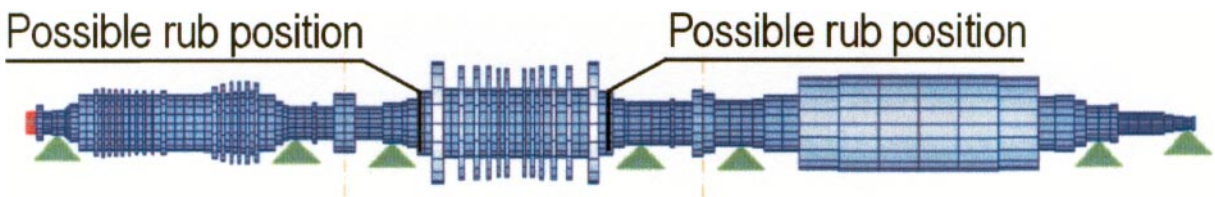

FIGURE 14
320 MW turbogenerator model used for unbalance identification.

TABLE 4
Rotor Pub Case: Experimental Critical Speeds for the Turbines and the Generator

	HP-IP turbine				LP turbine				Generator			
	1st		2nd		1st		2nd		1st		2nd	
	H	V	H	V	H	V	H	V	H	V	H	V
Rubbing turbogenerator	?	2020	?	?	1000	1460	2200	2870	833	?	1800	?
Similar turbogenerator	1300	1800	?	?	?	1440	?	>3000	1010	1215	2200	2800

maintenance, which indicated the rub in the sealing close to the LP last stage.

CONCLUSIONS

A multiple-model–based fault-identification method has been described, and two successful and interesting applications of the procedure, on experimental data from turbogenerators in power plants, have been shown. In the first case, data relative to a balancing on a 320 MW turbogenerator was used, and some considerations are presented regarding the choice of the rotating speed set for the identification. In the second case, the real machine, again a 320 MW turbogenerator but from a different manufacturer, presented a rub in a sealing, and the proposed method allowed identification of the position of the rub, as confirmed by subsequent maintenance inspection of the machine. In both cases, the proposed technique was effective in detecting the fault, even if the models of the machines were not fine-tuned, as often occurs in cases of real machines.

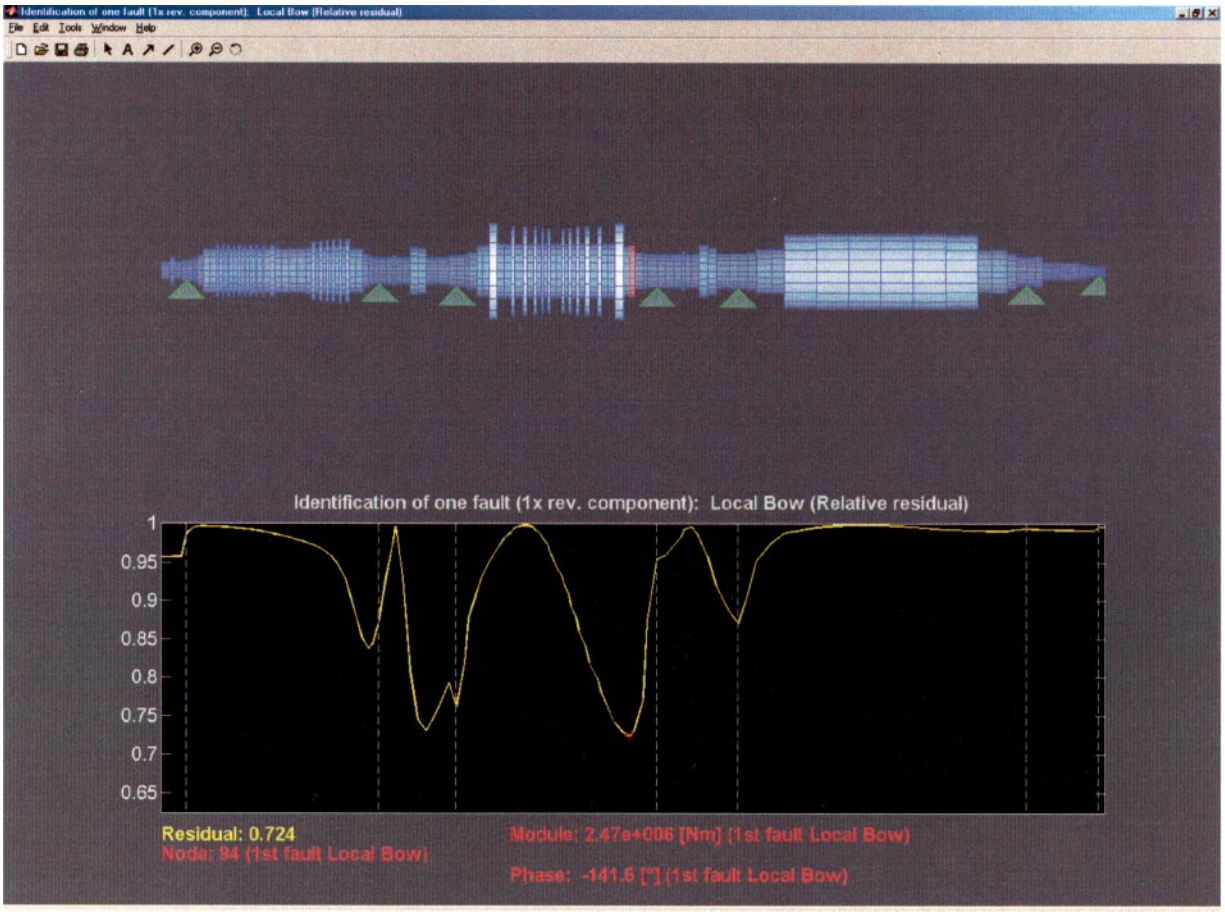

FIGURE 15
Residue along the rotor as calculated by ADVANT for a single rub.

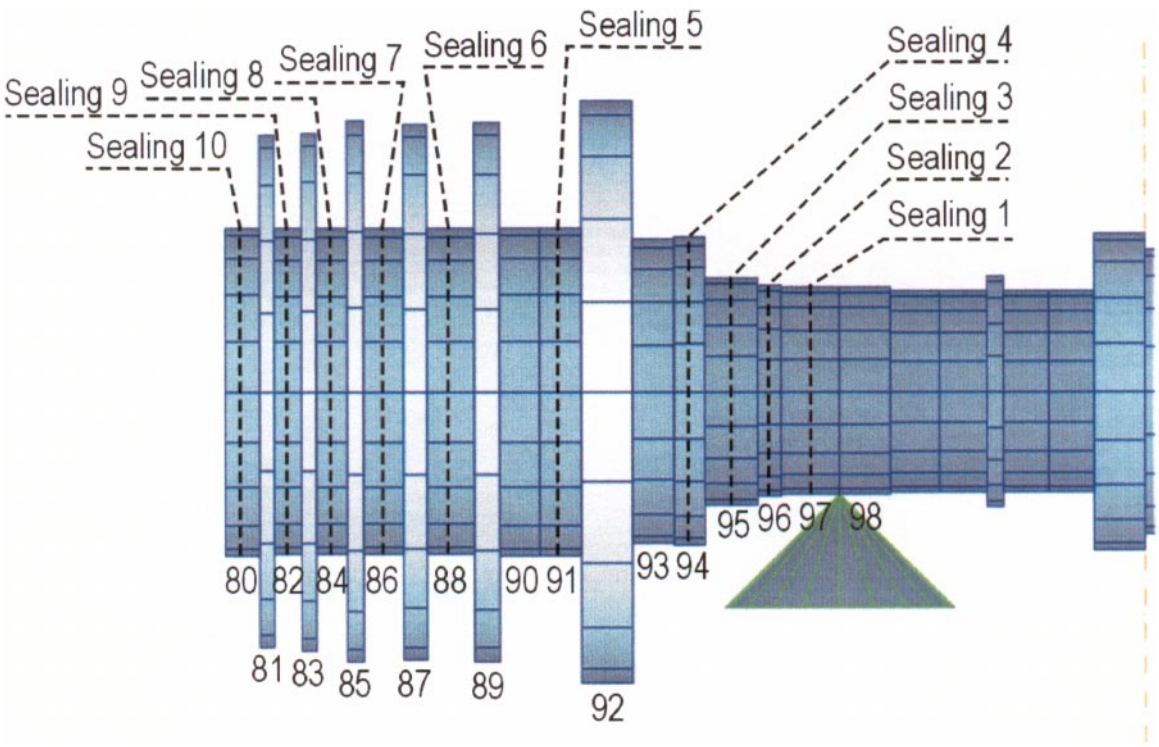

FIGURE 16
Sealing position on right hand side of the LP turbine.

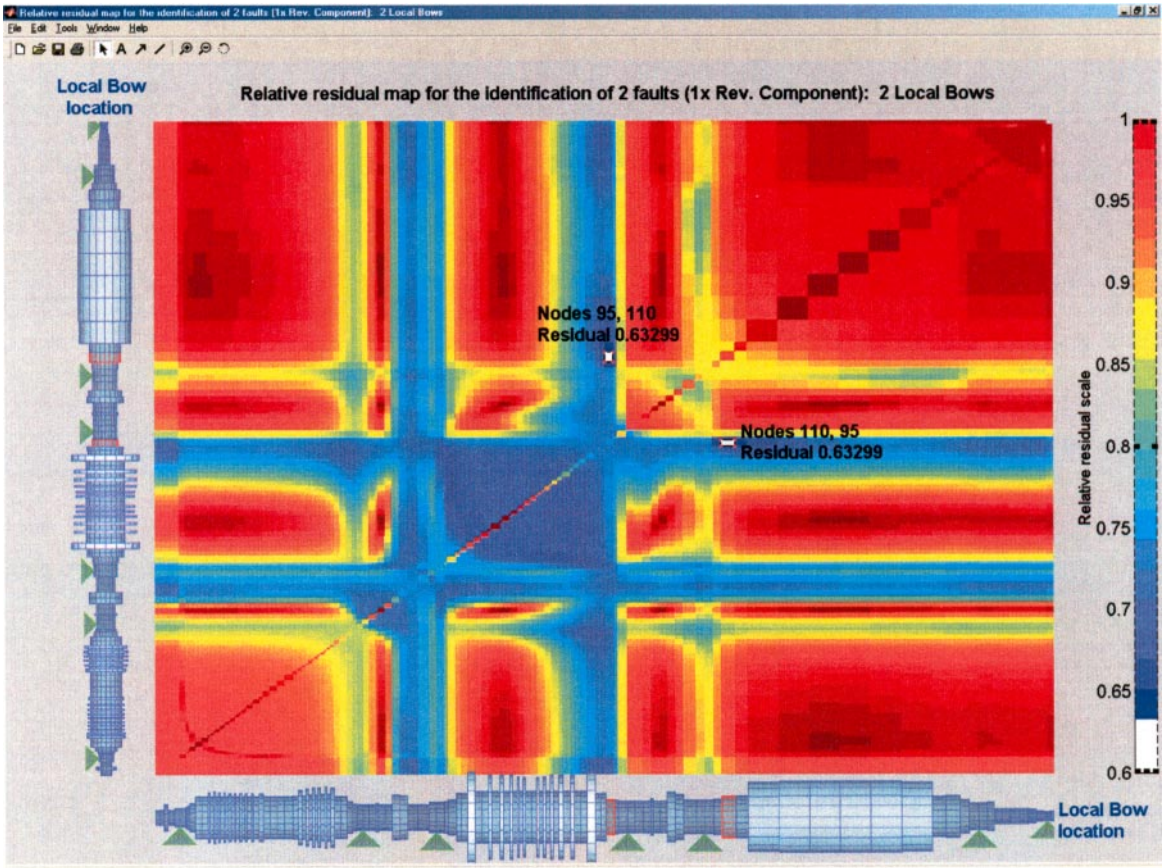

FIGURE 17
Residue map of the rotor as calculated by ADVANT for a double rub.

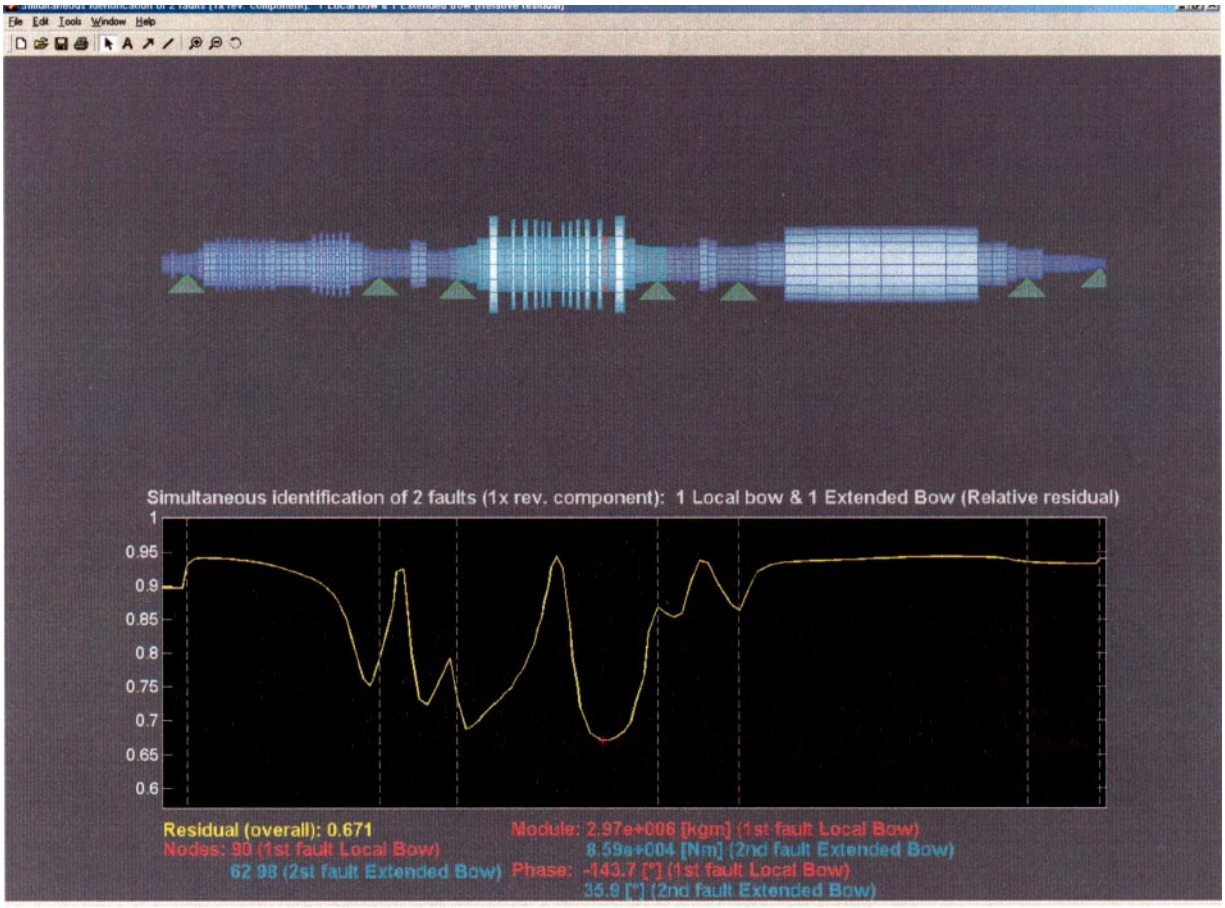

FIGURE 18
Residue along the rotor as calculated by ADVANT for a single rub and an extended bow.

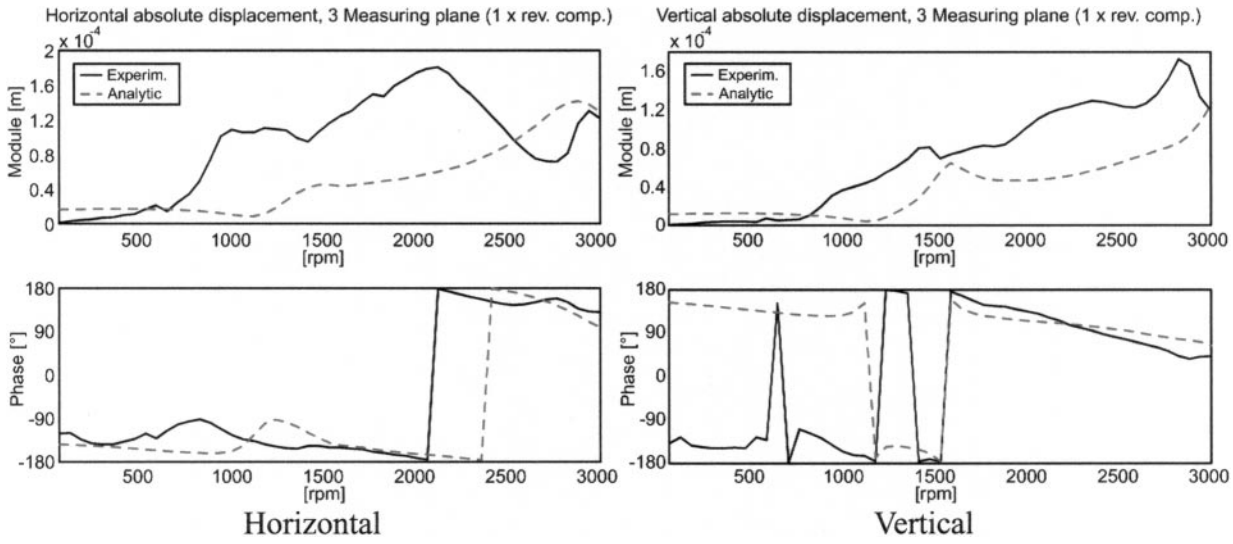

FIGURE 19
Rub and bow identification; comparison between experimental and calculated results for bearing 3.

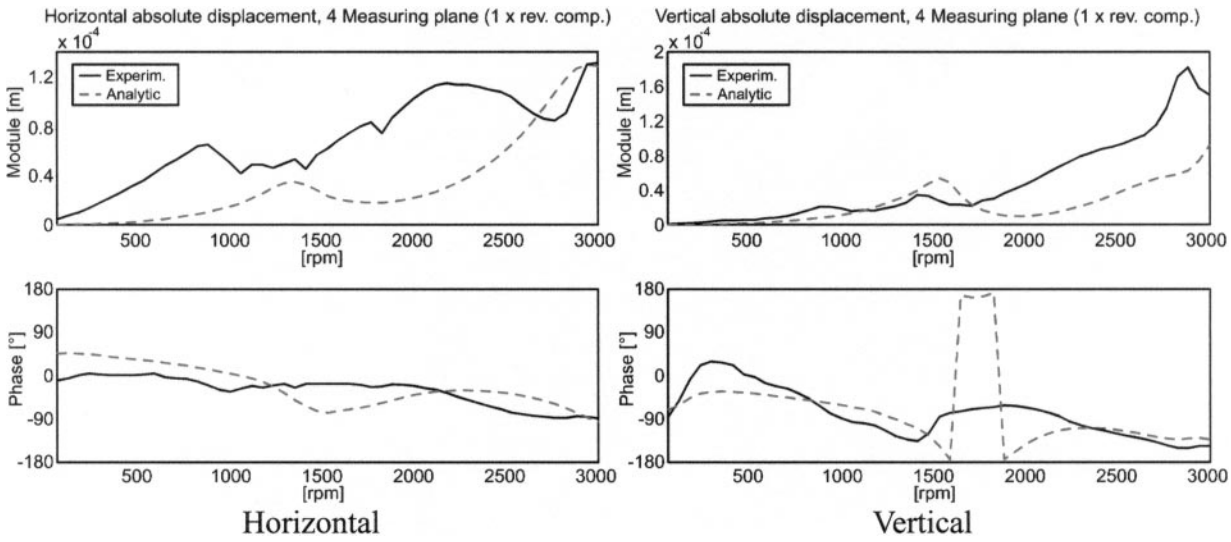

FIGURE 20
Rub and bow identification; comparison between experimental and calculated results for bearing 4.

NOMENCLATURE

$\mathbf{A}^{(k)}$	complex vector of the kth fault
$\mathbf{D}$	damping matrix
$d\mathbf{D}$	damping matrix change due to faults
$d\mathbf{K}$	stiffness matrix change due to faults
$d\mathbf{M}$	mass matrix change due to faults
$[\mathbf{E}(n\Omega)]$	system dynamical stiffness matrix
$\mathbf{F}$	force vector
$\mathbf{F}_f$	force vector due to faults
$\mathbf{F}_{fn}$	nth force vector harmonic component due to faults
$[\mathbf{F}_L^{(k)}]$	localization vector of the kth fault
F	force amplitude
$\mathbf{K}$	stiffness matrix
$\mathbf{M}$	moment vector, mass matrix
$\mathbf{M}_u$	original bow of the rotor
M	moment amplitude
m	number of faults, unbalance mass
n	number of the harmonic component
r	distance of the unbalance mass from the rotating axis
$\mathbf{U}$	original unbalance of the rotor
$\mathbf{W}$	rotor weight
$\mathbf{X}$	vector of vibration harmonic component
$\mathbf{X}_{An}$	partition of $\mathbf{X}_n$ for the nodes not corresponding to measuring points
$\mathbf{X}_{Bn}$	partition of $\mathbf{X}_n$ for the nodes corresponding to measuring points
$\mathbf{X}_n$	nth vibration harmonic component
$\mathbf{X}_{st}$	static deformation
$\mathbf{x}$	vibration due to fault only
$\mathbf{x}_t$	rotor total vibration
$\mathbf{x}_1$	vibration due to weight original unbalance and bow
z	rotor axial abscissa
α_n	inverse of $[\mathbf{E}(n\Omega)]$
α_{Bn}	partition of α_n for the nodes corresponding to measuring points
α_{An}	partition of α_n for the nodes not corresponding to measuring points
δ_n	difference between calculated and measured vibrations
δ_{rn}	relative residue
φ	phase
$\mathbf{\Omega}$	vector of rotating speeds
Ω	rotating speed, frequency

REFERENCES

Bachschmid, N., Vania, A., Tanzi, E., and Pennacchi, P. 1999, July. Identification and simulation of faults in rotor systems: experimental results, 3–11. *EURO DINAME 99: Dynamic Problems in Mechanics and Mechatronics, Wissenschaftszentrum Schloß Reisenburg der Universität Ulm*, Günzburg, Germany: University of Ulm.

Bachschmid, N., and Pennacchi, P. 2000, September. Model-based malfunction identification from bearing measurements, 571–580. *IMechE, 7th International Conference on Vibrations in Rotating Machinery*, 12–14. Nottingham, England: University of Nottingham.

Bachschmid, N., Pennacchi, P., and Audebert, S. 2000a, August. Some results in model-based transverse crack identification in rotor systems, xxx–xxx. *CONEM 2000, Congreso Nacional de Engenharia Mecànica*, Rio Grande do Norte, Brasil: Universitad Federal do Rio Grande do Norte.

Bachschmid, N., Pennacchi, P., Tanzi, E., and Audebert, S. 2000b, March. Identification of transverse cracks in rotors systems, 1065–1072. *ISROMAC-8 Conference*, Honolulu, Hawaii: Q16 bis.

Bachschmid, N., Pennacchi, P., Tanzi, E., and Vania, A. 2000c. Identification of transverse crack position and depth in rotor systems, 563–582. *Meccanica, International Journal of the Italian Association of Theoretical and Applied Mechanics* 35:(6)2000.

Bachschmid, N., Pennacchi, P., Tanzi, E., and Vania, A. 2000d. Accuracy of modelling and identification of malfunctions in rotor systems: